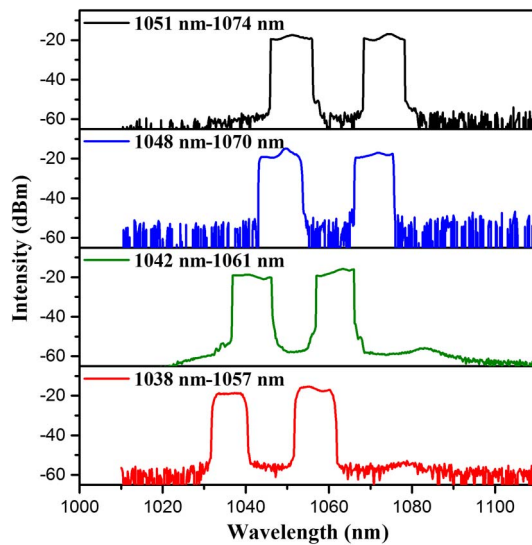


Tunable and Switchable Dual-Wavelength Dissipative Soliton Operation of a Weak-Birefringence All-Normal-Dispersion Yb-Doped Fiber Laser

Volume 5, Number 5, October 2013

Huaiqin Lin
Chunyu Guo
Shuangchen Ruan
Jinhui Yang
Deqin Ouyang
Yiming Wu
Liang Wen



DOI: 10.1109/JPHOT.2013.2281977
1943-0655 © 2013 IEEE

Tunable and Switchable Dual-Wavelength Dissipative Soliton Operation of a Weak-Birefringence All-Normal-Dispersion Yb-Doped Fiber Laser

Huaiqin Lin,^{1,2} Chunyu Guo,¹ Shuangchen Ruan,¹ Jinhui Yang,¹
Deqin Ouyang,^{1,2} Yiming Wu,^{1,2} and Liang Wen¹

¹Shenzhen Key Laboratory of Laser Engineering, Key Laboratory of Advanced Optical Precision Manufacturing Technology of Guangdong Higher Education Institutes, College of Electronic Science and Technology, Shenzhen University, Shenzhen 518060, China

²College of Optoelectronic Engineering, Shenzhen University, Shenzhen 518060, China

DOI: 10.1109/JPHOT.2013.2281977
1943-0655 © 2013 IEEE

Manuscript received July 17, 2013; revised August 26, 2013; accepted September 2, 2013. Date of publication September 16, 2013; date of current version September 24, 2013. This work was supported in part by the NSFC under Grants 61275144 and 61308049, by the PhD Start-Up Fund of Natural Science Foundation of Guangdong Province under Grant S2012040007242, by the Science and Technology Project of Shenzhen City under Grants JCYJ20120613110637373 and JCYJ20130329142022715, by the Natural Science Foundation of SZU under Grant 201203, and by the Improvement and Development Project of Shenzhen Key Lab under Grant ZDSY20120612094924467. Corresponding authors: C. Y. Guo and S. C. Ruan (e-mail: cyguo@szu.edu.cn; scruan@szu.edu.cn).

Abstract: We report on the generation of tunable and switchable dual-wavelength dissipative solitons (DSs) in a weak-birefringence all-normal-dispersion Yb-doped fiber laser based on the nonlinear polarization rotation technique. By virtue of the weak-birefringence operation, the switchable dual-wavelength DSs with a wide wavelength-tunable range and variable wavelength spacing are observed for the first time. The variable wavelength spacing is a result from the similar order of magnitude between the polarization controller-induced birefringence change and the fiber birefringence. It is suggested that a widely tunable wavelength spacing of the tunable and switchable dual-wavelength DSs could be realized through introducing an extra birefringence change whose magnitude is comparable with the fiber birefringence.

Index Terms: Fiber lasers, mode-locked lasers, tunable lasers and solitons.

1. Introduction

Recently, the dissipative soliton (DS) resonance characterized by a steep edge of spectrum and a great frequency chirp [1] has been intensively studied for its unique advantage of large pulse energy. Generally, the formation of DSs in fiber lasers is a result of mutual interactions among laser gain and loss, cavity dispersion, fiber nonlinear Kerr effect, and spectral filtering effect. The dynamics of the DSs is governed by the complex Ginzburg–Landau equation [2]. So far, the DS resonance has been achieved through diverse passively mode-locked techniques, including the semiconductor saturable absorption mirror [3], the carbon nanotube saturable absorber [4], the graphene mode locker [5], the nonlinear polarization rotation (NPR) [6], and the nonlinear amplifier loop mirror technique [7].

In addition, multi-wavelength mode-locked pulsed fiber lasers have attracted much attention owing to their versatile applications in optical fiber sensing, optical signal processing, and WDM

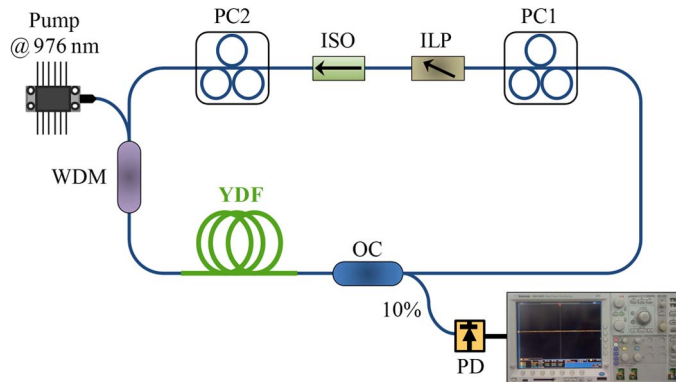


Fig. 1. Schematic diagram of the ANDi YDF laser. PC: polarization controller; ILP: in-line polarization; ISO: isolator; WDM: wavelength division multiplexer; YDF: Yb-doped fiber; OC: optical coupler; PD: photodetector.

optical fiber communications. It has been investigated that the birefringence-induced filtering effect can result in multiple soliton generation in passively mode-locked fiber lasers [8], [9]. Recently, the multi-wavelength DS has been generated in a Yb-doped fiber (YDF) laser based on a graphene-deposited tapered fiber device [10]. A switchable dual-wavelength mode-locked operation was demonstrated by exploiting a phase-shifted long-period fiber granting as a spectral filter in the laser cavity [11]. Whereas, owing to the wavelength position of the dual-wavelength output is determined by the passbands of the fiber granting filter, the output pulses cannot be wavelength-tuned. Moreover, Sova *et al.* have presented a tunable dual-wavelength laser in an all-PM fiber ring cavity [12]. Similarly, tunable and switchable dual-wavelength DS output can be also achieved by incorporating a section of polarization-maintaining fiber (PMF) which was to enhance the birefringence in the cavity [13]. However, the high-birefringence in the laser cavity fixes the wavelength spacing and is unfavorable to obtain a widely wavelength-tunable operation (only 7.7 nm), which is limited for some applications. The wavelength spacing of the dual-wavelength DS can be chosen only by changing the length of the PMF used in the cavity.

To the best of our knowledge, the tunable and switchable multi-wavelength DS operation with variable wavelength spacing has not been reported so far. In this paper, the tunable and switchable dual-wavelength DSs are generated in a weak-birefringence all-normal-dispersion (ANDi) YDF laser based on the NPR technique. Due to the weak-birefringence fiber utilized in the laser, the magnitude of the birefringence change induced by the rotation of the polarization controllers is close to that of the fiber birefringence. Consequently, the switchable dual-wavelength DSs not only have a wide wavelength-tunable range (17 nm) but also have variable wavelength spacing (19–23 nm).

2. Experimental Setup and Operation Principle

Fig. 1 shows the schematic diagram of the ANDi dual-wavelength DS fiber laser, which is based on the NPR technique. The gain medium is a 2.3-m single-mode YDF (Nufern) with a group-velocity dispersion (GVD) parameter of -43 ps/nm/km at 1060 nm and an absorption coefficient of 250 dB/m at 976 nm. It is pumped by a 976-nm laser diode (LD) through a 980-/1060-nm WDM. The rest of the fibers, including the tail fibers of each optical component and the twisted fibers in the PCs, are all standard single-mode fibers (HI-1060) with a GVD parameter of -38 ps/nm/km at 1060 nm. The total cavity length and the calculated cavity dispersion at 1060 nm are 8.5 m and 0.20 ps^2 , respectively. An isolator (ISO) is used in the cavity to force the unidirectional operation of the ring, and a pair of polarization controllers (PC1 and PC2) are inserted to fine tune the linear-cavity birefringence. In addition, two PCs, together with an in-line polarizer (ILP), are utilized to generate the birefringence-induced filtering effect. Then a 1×2 optical coupler (OC) is used to couple about 10% of the circulating power out of the cavity. The output laser is monitored by an optical spectrum analyzer (Yokogawa AQ6370B), a radio-frequency (RF) spectrum analyzer (Tektronix RSA

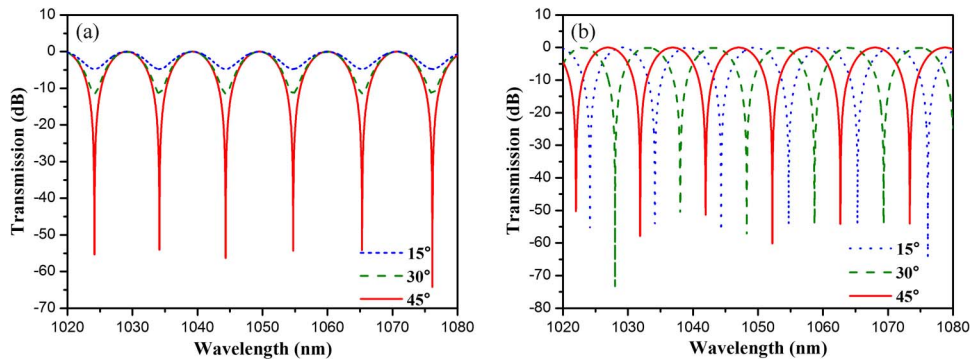


Fig. 2. Simulated transmission spectra of the birefringence-induced filtering effect.

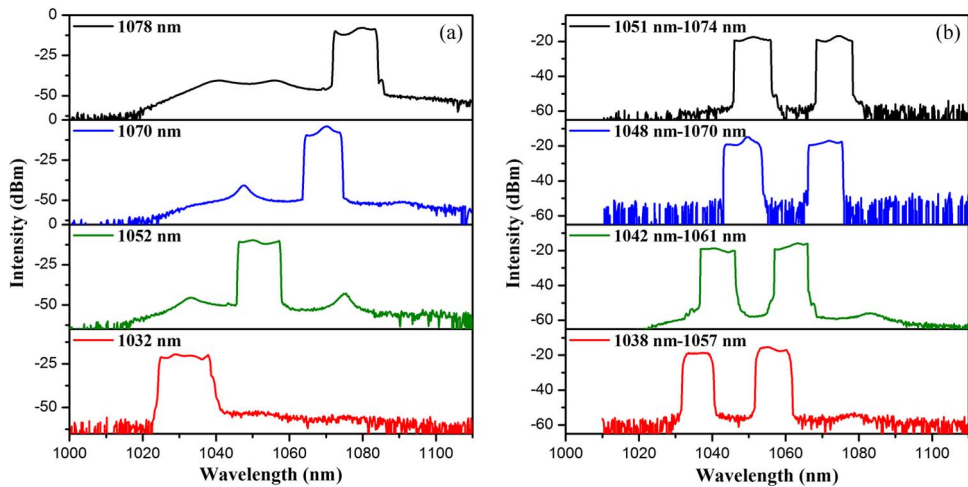


Fig. 3. (a) Tunable single-wavelength DSs from 1032 to 1078 nm and (b) tunable dual-wavelength DSs with variable wavelength spacing.

3303B), an autocorrelator (APE, PulseCheck SM), and a 350-MHZ oscilloscope (Tektronix MSO 4032) together with a 1.5-GHz photodetector simultaneously.

As aforementioned, since an ILP and two PCs were used, the birefringence-induced filtering effect could be generated in the fiber laser. The transmission function of the birefringence-induced filtering effect [14], [15] is numerically investigated. Fig. 2 shows the simulation results of the periodical transmission distribution with respect to the wavelength [14]. As shown in Fig. 2(a), the extinction ratio of the filter is determined by the ratio of light coupled into the slow and fast axes of the fiber and is maximized when the coupling ratio is 50:50. Moreover, the change of the angles between the polarization direction and the fast axis of the fiber allows the shifting of the transmission peak wavelength and a constant filter bandwidth, as shown in Fig. 2(b). Thus, the transmission peak wavelength can be controlled by the PCs. In addition, the peak wavelength spacing ($\Delta\lambda$) is decided by the formula $\lambda^2(\Delta nL)$, where λ is the central wavelength, L is the cavity length, and Δn is the strength of birefringence.

3. Experimental Results and Discussions

Experimentally, with appropriate adjustment of the PCs, tunable single-wavelength DSs and dual-wavelength DSs can be achieved, respectively. The threshold for the self-started mode-locked operation of the fiber laser is 230 mW. In the experiment, the pump power is set to 250 mW to optimize the laser performance. Fig. 3(a) shows the output spectra of the tunable single-wavelength

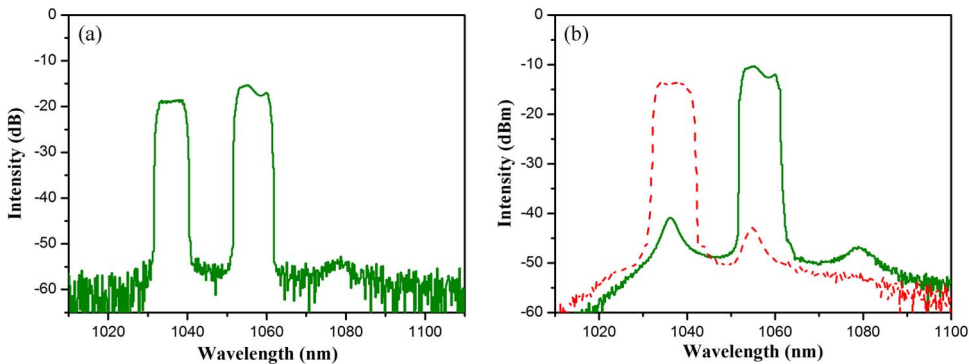


Fig. 4. (a) Dual-wavelength DS operation at 1038 and 1057 nm and (b) the corresponding switchable dual-wavelength DS operation.

DSs, with a wavelength-tunable range from 1032 to 1078 nm and a variable edge-to-edge bandwidth from 15.4 to 10.8 nm. During the whole tunable range, the pulse duration has no remarkable variation and retains as short as 10.2 ps (Gaussian profile assumed). This pulse duration and a 3-dB spectrum bandwidth of 5 nm give rise to a time-bandwidth product of 13.5, indicating that the pulses are strongly chirped. It is also visible that the spectra exhibit steep edges, which is the typical feature of the DSs in ANDi lasers.

Moreover, stable dual-wavelength DSs can be achieved by carefully adjusting the orientation of the PCs, as shown in Fig. 3(b). In contrast to the high-birefringence cavity described in reference [13], we get a wider wavelength-tunable range of 17 nm without an additional PMF. In particular, the wavelength spacing of the dual-wavelength DSs can vary from 19 to 23 nm, whereas it is fixed in the high-birefringence cavity.

The dual-wavelength DS operation at 1038 and 1057 nm is further discussed, as shown in Fig. 4(a). The edge-to-edge bandwidths of two separated mode-locked pulse spectra are 8.6 and 10 nm, respectively. Due to the effect of mode competition, the bandwidths of the two separated mode-locked pulse spectra are narrower than that of the single-wavelength mode-locked pulse spectrum. In this case, according to the wavelength spacing of 19 nm, the birefringence in the cavity is calculated to be as low as 6×10^{-6} based on the aforementioned formula. It presents evidence that the non-PM cavity elements can effectively function as unintended filters in the cavity. In addition, the birefringence change induced by the rotation of the PCs is estimated to be an order of magnitude of 10^{-7} . According to the aforementioned formula, the relationship between the wavelength spacing change ($\Delta\lambda'$) and the birefringence change ($\Delta n'$) can be described as $\Delta\lambda' = \Delta\lambda - \lambda^2/[(\Delta n - \Delta n')L]$. Consequently, in the high-birefringence ($\sim 10^{-4}$) cavity, this little birefringence change is negligible, and thus, the wavelength spacing is fixed. More importantly, it is suggested that a widely tunable wavelength spacing of these dual-wavelength DSs could be realized by introducing an extra birefringence change whose magnitude is comparable with the fiber birefringence.

It is worth mentioning that the tunable dual-wavelength DSs also have an anticipative switchability. As shown in Fig. 4(b), the spectrum of mode-locked operation at 1038 nm is accompanied with a sideband at 1056 nm (red curve). After the laser had realized the mode-locked operation at 1038 nm, with one paddle of the PCs tuned along a required orientation coherently, the sideband intensity is gradually strengthened and the mode-locked operation finally turns to be at 1057 nm (green curve). This evolution is reversible. It can be noted that both the two states between the mode-locked operation and the sideband operation at one wavelength are exchangeable.

Furthermore, the characteristic of the dual-wavelength DS operation at 1038 and 1057 nm is further investigated. The oscilloscope traces for the two mode-locked pulses are shown in Fig. 5(a), and there is no evident discrepancy between them due to the limited response time of the photodetector. Only a naked-eye observation of amplitude jump happened when the mode-locked spectrum turns from one to the other. Accordingly, the output power of the 1038- and 1057-nm

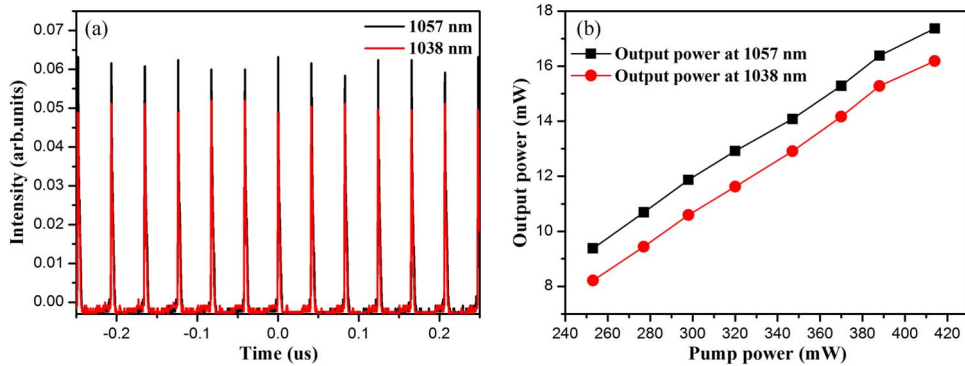


Fig. 5. (a) Oscilloscope traces for two mode-locked pulses. (b) output power of the dual-wavelength DSSs versus pump power at 1038 and 1057 nm.

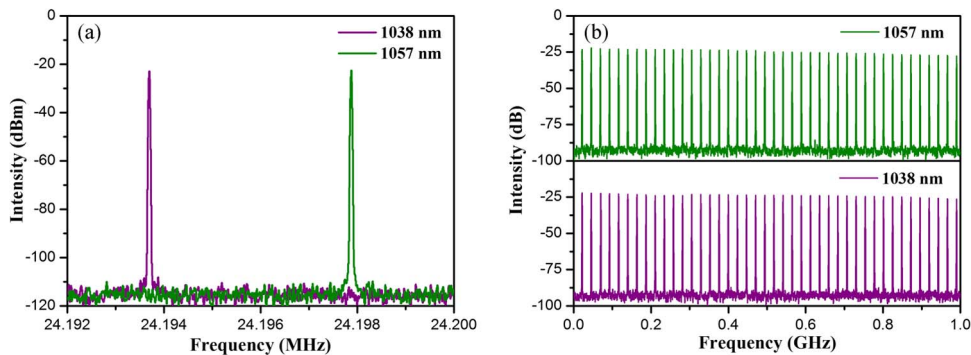


Fig. 6. RF spectrum (a) around the fundamental and (b) harmonic repetition rates at 1038 and 1057 nm.

mode-locked pulses is separately measured, as shown in Fig. 5(b). The maximum output powers are 17.4 and 16.2 mW, with the corresponding slope efficiencies of 4.97% and 5.04%, respectively. The further scaling of the output power is primarily limited by the available pump power of 410 mW. In fact, the relative intensity of the operation at the two wavelengths is varied with the orientation of the PCs. It is because that the transmission function of the laser cavity with respect to wavelength is related to the orientation of the PCs.

Fig. 6 shows the RF spectra of the two mode-locked pulses around the fundamental and harmonic repetition rates with a span range of 1 GHz. The resolution bandwidths are 20 Hz and 20 kHz, respectively. As shown in Fig. 6(a), the round-trip frequency for 1038 and 1057 nm are 24.1938 and 24.1979 MHz, respectively. Thus, the spacing (Δf) between the two RF spectra is 4.1 kHz. The relationship between the wavelength difference and RF spacing can be theoretically analyzed, as described in [16] and [17]. Here, $c = 3 \times 10^8$ m/s, $n = 1.46$, $D_{\text{SMF+YDF}} \approx -41$ ps/nm/km, $L = 8.5$ m, and $\Delta\lambda = 19$ nm. Consequently, the theoretical result of Δf can be calculated as 3.9 kHz, which well confirms the experimental observations. In addition, the excellent mode-locked stability and the low pulse energy fluctuation at these two wavelengths are indicated from the 85-dB signal-to-noise ratio.

Fig. 7(a) shows the autocorrelation trace of the synchronized dual-wavelength DSSs. The pulse duration is as short as 15.4 ps with a Gaussian profile. Compared with the single-wavelength DS operation, the pulse duration of the dual-wavelength DSSs becomes broader due to the auto-correlation superposition of the pulses at two wavelengths. Furthermore, the autocorrelation traces of the separated dual-wavelength DSSs are shown in Fig. 7(b). It can be seen that the pulse durations are 11.3 ps (at 1038 nm) and 14.2 ps (at 1057 nm), respectively.

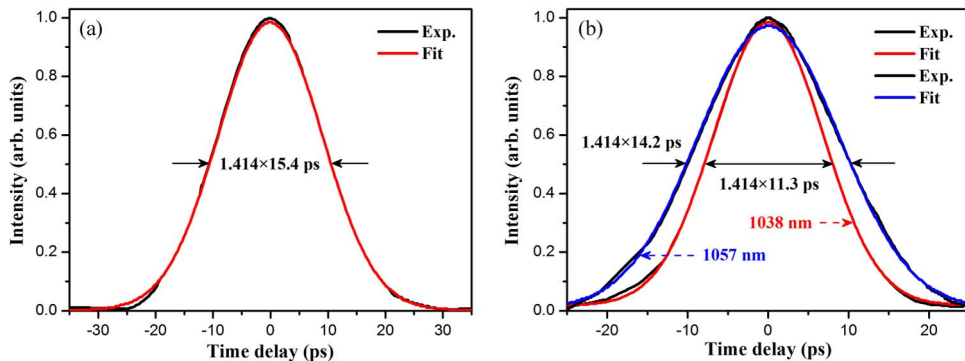


Fig. 7. Autocorrelation traces of (a) the synchronized dual-wavelength DSs and (b) the separated dual-wavelength DSs at 1038 nm and 1057 nm.

4. Conclusion

In conclusion, we have demonstrated the tunable and switchable dual-wavelength DS generation from a weak-birefringence ANDi YDF laser based on the NPR technique. The switchable dual-wavelength DSs with a wide wavelength-tunable range (17 nm) and variable wavelength spacing (19–23 nm) are realized for the first time. A magnitude of 10^{-7} of the birefringence change induced by the rotation of the PCs is also demonstrated. It is suggested that a widely tunable wavelength spacing of the tunable and switchable dual-wavelength DSs could be realized through introducing an extra birefringence change whose magnitude is comparable with the fiber birefringence. Such an all-fiber DS laser may find applications in optical signal processing or WDM optical fiber systems.

References

- [1] L. M. Zhao, D. Y. Tang, X. Wu, D. J. Lei, and S. C. Wen, "Bound states of gain-guided solitons in a passively mode-locked fiber laser," *Opt. Lett.*, vol. 32, no. 21, pp. 3191–3193, Nov. 2007.
- [2] N. Akhmediev, J. M. Soto-Crespo, and G. Town, "Pulsating solitons, chaotic solitons, period doubling, and pulse coexistence in mode-locked lasers: Complex Ginzburg-Landau equation approach," *Phys. Rev. E, Stat. Nonlin. Soft Matter Phys.*, vol. 63, no. 5, pp. 056602-1–056602-13, Apr. 2001.
- [3] H. Zhang, D. Y. Tang, L. M. Zhao, X. Wu, and H. Y. Tam, "Dissipative vector solitons in a dispersion-managed cavity fiber laser with net positive cavity dispersion," *Opt. Exp.*, vol. 17, no. 2, pp. 455–460, Jan. 2009.
- [4] J. H. Im, S. Y. Choi, F. Rotermund, and D. I. Yeom, "All-fiber Er-doped dissipative soliton laser based on evanescent field interaction with carbon nanotube saturable absorber," *Opt. Exp.*, vol. 18, no. 21, pp. 22 141–22 146, Oct. 2010.
- [5] L. M. Zhao, D. Y. Tang, H. Zhang, X. Wu, Q. Bao, and K. P. Loh, "Dissipative soliton operation of an ytterbium-doped fiber laser mode locked with atomic multilayer graphene," *Opt. Lett.*, vol. 35, no. 21, pp. 3622–3624, Nov. 2010.
- [6] C. M. Ouyang, P. P. Shum, K. Wu, J. Wong, X. Wu, H. Q. Lam, and S. Aditya, "Dissipative soliton (12 nJ) from an all-fiber passively mode-locked laser with large normal dispersion," *IEEE Photon. J.*, vol. 3, no. 5, pp. 881–887, Oct. 2011.
- [7] S. K. Wang, Q. Y. Ning, A. P. Luo, Z. B. Lin, Z. C. Luo, and W. C. Xu, "Dissipative soliton resonance in a passively mode-locked figure-eight fiber laser," *Opt. Exp.*, vol. 21, no. 2, pp. 2402–2407, Jan. 2013.
- [8] C. J. Chen, P. K. A. Wai, and C. R. Menyuk, "Soliton fiber ring laser," *Opt. Lett.*, vol. 17, no. 6, pp. 417–419, Mar. 1992.
- [9] D. Y. Tang, L. M. Zhao, B. Zhao, and A. Q. Liu, "Mechanism of multisoliton formation and soliton energy quantization in passively mode-locked fiber lasers," *Phys. Rev. A, At. Mol. Opt. Phys.*, vol. 72, no. 4, pp. 043816-1–043816-4, Oct. 2005.
- [10] Z. Luo, Y. Huang, J. Wang, H. Cheng, Z. Cai, and C. Ye, "Multiwavelength dissipative-soliton generation in Yb-fiber laser using graphene-deposited fiber-taper," *IEEE Photon. Technol. Lett.*, vol. 24, no. 17, pp. 1539–1542, Sep. 2012.
- [11] X. J. Zhu, C. H. Wang, S. X. Liu, D. F. Hu, J. J. Wang, and C. Y. Zhu, "Switchable dual-wavelength and passively mode-locked all-normal-dispersion Yb-doped fiber lasers," *IEEE Photon. Technol. Lett.*, vol. 23, no. 14, pp. 956–958, Jul. 2011.
- [12] R. M. Sova, C. S. Kim, and J. U. Kang, "Tunable dual-wavelength all-PM fiber ring laser," *IEEE Photon. Technol. Lett.*, vol. 14, no. 3, pp. 287–289, Mar. 2012.
- [13] Z. X. Zhang, Z. W. Xu, and L. Zhang, "Tunable and switchable dual-wavelength dissipative soliton generation in an all-normal-dispersion Yb-doped fiber laser with birefringence fiber filter," *Opt. Exp.*, vol. 20, no. 24, pp. 26 736–26 742, Nov. 2012.

- [14] M. X. Wang, J. Wu, and J. Lin, "Multiwavelength fiber ring laser based on an SOA and Lyot birefringent filter," in *Proc. SPIE, Passive Compon. Fiber-based Devices*, Nov. 2008, vol. 7134, pp. 7134L-1–7134L-8.
- [15] K. Özgören and F. Ö. Ilday, "All-fiber all-normal dispersion laser with a fiber-based Lyot filter," *Opt. Lett.*, vol. 35, no. 8, pp. 1296–1298, Apr. 2010.
- [16] G. P. Agrawal, *Nonlinear Fiber Optics* 3rd ed., San Diego, CA, USA: Academic, 2001.
- [17] L. Yun, X. M. Liu, and D. Mao, "Observation of dual-wavelength dissipative solitons in a figure-eight erbium-doped fiber laser," *Opt. Exp.*, vol. 20, no. 19, pp. 20 992–20 997, Sep. 2012.